Journal of Ceramic Processing Research. Vol. 25, No. 4, pp. 664~672 (2024)
(Received 15 May 2024, Received in revised form 17 July 2024, Accepted 31 July 2024)
https://doi.org/10.36410/jcpr.2024.25.4.664

J O U R N A L O F
Ceramic Processing Research

CO_2 capture performance optimization of MgO-based adsorbent modified by alkali metal salt

Yufei Sun, Qiuwan Shen*, Xin Zhang, Gaokui Chen, Kuanyu Zhu and Shian Li
Marine Engineering College, Dalian Maritime University, Dalian, China

With the increasingly serious problem of climate warming in recent years, CO_2 capture technology has been widely concerned by countries all over the world. One of the effective methods to reduce CO_2 emissions is to capture CO_2 after combustion. Alkali metal salt modified MgO-based adsorbents were synthesized by hydration impregnation method to obtain high efficient adsorbents in this study. The CO_2 cyclic adsorption capacity test was carried out in a fixed bed experimental setup. The microstructure of the adsorbent was characterized by XRD, SEM and BET techniques. The adsorption properties and cycle stability of alkali metal salts modified MgO adsorbents were deeply studied. The results show that the adsorbent with 10 wt% K_2CO_3-MgO has the best adsorption performance and cyclic stability. The initial adsorption capacity is 89 mg/g·sorbent, and the adsorption capacity of the 15th cycle is 63 mgCO_2/ g·sorbent. 10 wt% K_2CO_3-MgO adsorbent has the largest specific surface area, and K_2CO_3 doping of alkali metal carbonate can effectively improve the CO_2 adsorption capacity and cyclic stability of the adsorbent.

Keywords: CO_2 adsorbent, MgO, Alkali metal salt, Adsorption capacity, Cyclic stability.

Introduction

The majority of global carbon dioxide emissions come from coal-fired power plants and the transportation industry, making effective capture of this carbon dioxide a focal point of concern for governments, businesses, and academia both domestically and internationally. Within the existing coal-fired power systems, CO_2 capture at coal-fired plants primarily follows three routes: pre-combustion capture, post-combustion capture, and oxy-fuel combustion [1-5]. Figure 1 shows the post-combustion carbon capture process using MgO as an adsorbent. MgO captures CO_2 through cyclic carbonation/ calcination process, and the following is the reaction equation.

$$MgO + CO_2 \rightarrow MgCO_3 \quad (1)$$

$$MgCO_3 \rightarrow MgO + CO_2 \quad (2)$$

However, the practical application of pure MgO is greatly limited due to its low CO_2 adsorption capacity and poor stability in adsorption-regeneration cycles [6]. Consequently, it is necessary to modify MgO to enhance its CO_2 adsorption performance.

Currently, research on enhancing the CO_2 adsorption capacity of MgO often involves altering its microstructure or incorporating a second metal oxide to modify its properties. Despite its high theoretical adsorption capacity, the continuous reaction of MgO with CO_2 leads to the formation of a dense layer of $MgCO_3$ on its surface, which inhibits further reactions and results in a very low adsorption capacity of pure MgO. The CO_2 adsorption capacity of commercial pure MgO ranges only from 0.0092 to 0.018 g/g [7]. To improve the adsorption ability of pure MgO, it is crucial to increase its specific surface area and pore volume and to reduce the impact of $MgCO_3$ formation on its CO_2 adsorption performance. Song et al. [8] synthesized MgO with varying microstructures by calcining different precursors (magnesium hydroxide, basic magnesium carbonate, and magnesium oxalate). Their results demonstrated that MgO derived from these precursors had significantly increased surface areas and pore volumes. Specifically, MgO obtained from magnesium hydroxide exhibited the largest specific surface area at 211.3 m^2/g, while that derived from magnesium oxalate had the largest pore volume at 0.484 m^3/g and also showed the highest CO_2 adsorption capacity at 0.061 g/g. Hanif et al. [9] produced nanoscale MgO with high surface area and large pore volume by calcining samples under vacuum at 400°C using ammonia as a precipitant, achieving a CO_2 adsorption capacity of 0.088 g/g at 200°C. Han et al. [10] employed a sol-gel process combined with supercritical CO_2 drying to prepare a series of nanoscale MgO-based CO_2 adsorbents. At a calcination temperature of 600°C, as the Mg/Al molar ratio varied from 0 to

*Corresponding author:
Tel : +98-833-37296591
Fax: +98-833-38277164
E-mail: roholahsharifi@gmail.com

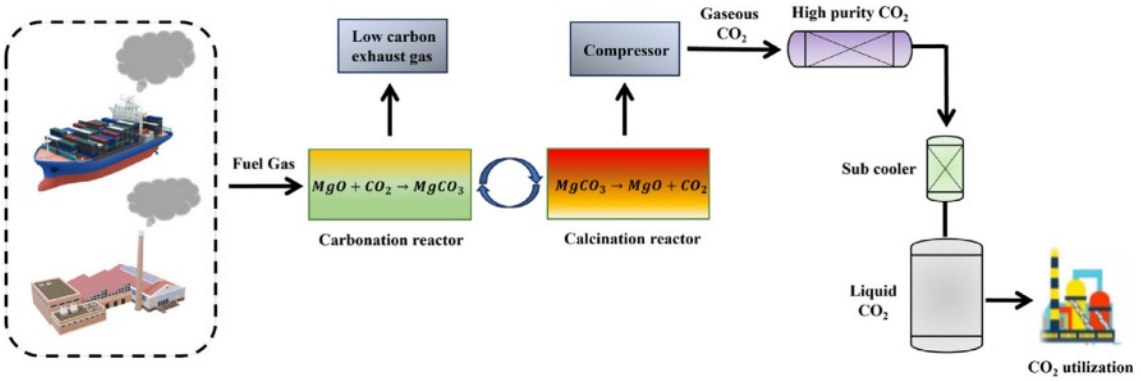

Fig. 1. Post-combustion capture process using MgO adsorbent.

3, the composition of the adsorbent transitioned from Al_2O_3 to $MgAl_2O_4$ through $MgAl_2O_3$. The adsorbent with a Mg/Al molar ratio of 0.5 exhibited a surface area of 409 m^2/g and a pore volume of 1.4 cm^3/g, and under conditions of 200 °C and 10% CO_2, its adsorption capacity was approximately 0.026 g/g. Li et al. [11] used a wet impregnation method to load magnesium acetate tetrahydrate and magnesium nitrate hexahydrate onto various carriers such as activated carbon and silica. The results indicated that the carbonization of magnesium acetate tetrahydrate prevented the agglomeration of MgO, thus enhancing the dispersion and consequently, the CO_2 adsorption performance of MgO/SiO_2 adsorbents. However, despite these modifications to MgO's microstructure or the incorporation of a second metal oxide, the CO_2 adsorption capacity of modified MgO adsorbents remains relatively low, and their suitable temperature range is narrow. Recently, some researchers have started incorporating alkali metal nitrates or carbonates to modify MgO, which not only improves its CO_2 adsorption capacity but also extends the applicable temperature range for CO_2 adsorption. Xiao et al. [12] modified MgO with K_2CO_3 and investigated the impact of the Mg/K molar ratio on the adsorbent's CO_2 adsorption capability. The results showed that at an adsorption temperature of 350°C and 100% CO_2, the highest adsorption capacity was achieved with a Mg/K molar ratio of 1:1.89. Hatton et al. [13] coated basic magnesium carbonate with a layer of mixed nitrates and then examined the effects of the composition of mixed nitrates, carbonation temperature, and nitrate loading on CO_2 adsorption capacity. The findings indicated that the 15 mol% (Li-Na-K)NO_3/MgO adsorbent did not decrease in adsorption capacity even after 40 adsorption-regeneration cycles; instead, it increased.

Therefore, the purpose of this study is to modify MgO with alkali metal salts to enhance its adsorption capacity for CO_2. By modifying MgO with chloride salt and carbonates, it is aimed to improve both the CO_2 adsorption performance and the cyclic stability of MgO-based adsorbent. In this study, the influence of different types of alkali metal salts and their mass ratios on the CO_2 adsorption performance of MgO was investigated. All adsorbents are prepared using a hydration impregnation method, and CO_2 adsorption tests are conducted in a fixed-bed reactor. In addition, the adsorbent underwent multiple cyclic adsorption and regeneration experiments, and the cyclic CO_2 adsorption capacity was analyzed and discussed.

Experimental Results

Preparation method

In this study, hydration impregnation method was used to prepare MgO-based adsorbent. Firstly, calcine pure MgO in a muffle furnace at 650°C for 3 hours. Then, mix the calcined MgO thoroughly in a solution containing 80ml of alkali metal ions. Then heat the obtained mixture in a water bath at 80°C and stir continuously for 3 hours until the water has almost evaporated. Afterwards, dry the evaporated paste mixture in a drying oven at 100°C for 12 hours. Finally, remove and grind it to obtain the final powder sample. The mass ratio of each substance and the sample naming of the adsorbent are shown in Table 1.

CO_2 Cyclic Adsorption Experiment

The cyclical CO_2 capture performance of MgO-based adsorbent was studied in a fixed bed reactor. As shown in Fig. 2.

Table 1. Synthesized MgO-based adsorbents.

Serial number	Sample named	Mass ratio
1	MgO	Pure MgO
2	KCl-4MgO	KCl:MgO=1:4
3	KCl-9MgO	KCl:MgO=1:9
4	NaCl-9MgO	NaCl:MgO=1:9
5	NaCl-4MgO	NaCl:MgO=1:4
6	K_2CO_3-9MgO	K_2CO_3:MgO=1:9
7	K_2CO_3-4MgO	K_2CO_3:MgO=1:4
8	Na_2CO_3-9MgO	Na_2CO_3:MgO=1:9
9	Na_2CO_3-4MgO	Na_2CO_3:MgO=1:4

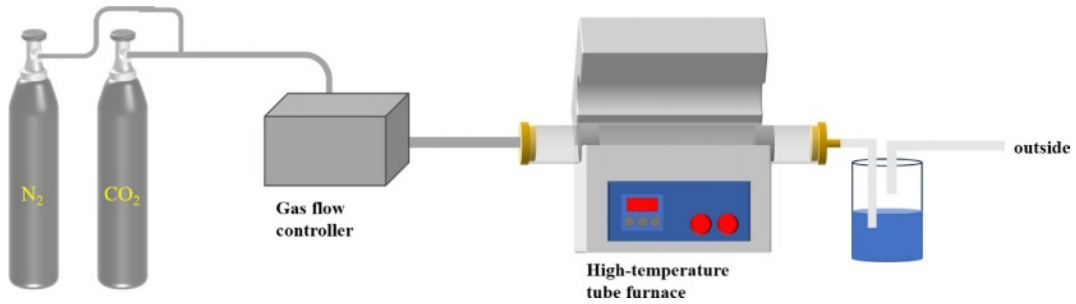

Fig. 2. Diagram of the fixed-bed CO_2 cyclic adsorption experimental setup.

The calcination temperature was 500°C, and the calcination time was 15 min under the pure N_2 atmosphere. The carbonation temperature is 380°C and the carbonation time is 15 min. Firstly, the adsorption capacity and cycle stability of 9 groups of samples were tested by 5 adsorption-desorption cycles. Among them, 4 groups of samples with better adsorption performance and cycle stability were added to 10 cycles, and the cycle process was consistent with the atmosphere. Four groups of carbonate modified samples were calcined at 280°C, 330°C and 380°C for five cycles in order to explore the influence of temperature on the cyclic adsorption performance of adsorbents. The adsorbent is firstly calcined at high temperature, $MgCO_3$ or $Mg(OH)_2$ is completely decomposed into MgO, and the calcined adsorbent is carbonated. The mass of calcined and carbonated adsorbent samples was weighed by electronic balance, and the CO_2 adsorption capacity (C_n) was calculated by the change of sample mass. The performance of cycling CO_2 capture was evaluated by this parameter, and the calculation formula was shown in Formula (1). The precision of electronic balance is 1mg, and the balance error is relatively small. Moreover, the average value is taken as experimental data after many measurements in numerical processing, and the result is more accurate.

$$C_n = \frac{m_n - m_{n-1}}{m_o} \tag{3}$$

Where n is the number of cyclic reactions; C_n is the adsorption amount of CO_2 after the nth cycle, representing the mass of CO_2 adsorbed by the calcined adsorbent per unit mass, and the unit is mg/g; m_n is the mass of adsorbent after the nth cycle, and the unit is mg; m_{n-1} is the mass of the sample after the calcination stage of the (n-1) cycle, and the unit is mg; m_0 is the mass of adsorbent after initial calcination, and the unit is g.

Characterization

Ultima IV X-ray diffractometer made by Rigaku Company of Japan was used to determine the phase and analyze the crystal phase of the adsorbent. Using copper target, the sample was laid on a glass slide and placed in the X-ray diffractometer. The scanning range was 10° ~90°, and the scanning speed was 5°/min.

SUPRA 55 SAPPHIRE field emission scanning electron microscope produced by ZEISS Company of Germany was used to analyze the appearance and element distribution of the samples. Scanning electron microscope (SEM) was imaged by backscattered electron beam or secondary electron, and gold was sprayed for 150s under vacuum condition before testing. The amplification factor is 10~100 K, and the acceleration voltage is 5~20 KV.

The adsorbents were adsorbed and desorbed by ASAP 2460 automatic specific surface area and porosity analyzer produced by Micromeritics Company of USA. The specific surface area and pore characteristics of adsorbents were analyzed by multi-molecular layer adsorption theory and pore size distribution calculation model.

Results and Discussion

Comparison experiment of the adsorbent performance

The CO_2 adsorption performance of MgO based adsorbents modified with different alkali metal salts (K_2CO_3, Na_2CO_3, KCl, NaCl) at 380°C was compared. The result is shown in Fig. 3. It can be seen that K_2CO_3, Na_2CO_3, and NaCl modified MgO adsorbents have better initial CO_2 adsorption performance than unmodified pure MgO, and the adsorption performance of these adsorbents will decrease to varying degrees with increasing cycle times. Figs. 3(a)~(d) show a comparison of MgO and modified adsorbents with different mass ratios. In the first cycle, all adsorbents except KCl-9MgO have good CO_2 capture capacity, with CO_2 adsorption capacity above 58 mg/g·adsorbent. Among them, K_2CO_3-9MgO adsorbent has the best adsorption performance, with a first adsorption capacity of 89 mg/g·adsorbent. As the number of cycles increases, the adsorption capacity of all adsorbents for CO_2 decreases to varying degrees. Among them, the adsorption capacity of NaCl-9MgO and NaCl-4MgO adsorbents decreased significantly, and their cycling stability was poor. After the fifth cycle, the adsorption capacity decreased to approximately 25 mg/g·adsorbent and 17 mg/g·adsorbent, respectively. And K_2CO_3-9MgO and Na_2CO_3-4MgO adsorbents exhibit strong cyclic adsorption capacity. After the fifth cycle, the adsorption capacity of CO_2 can still reach 71.9

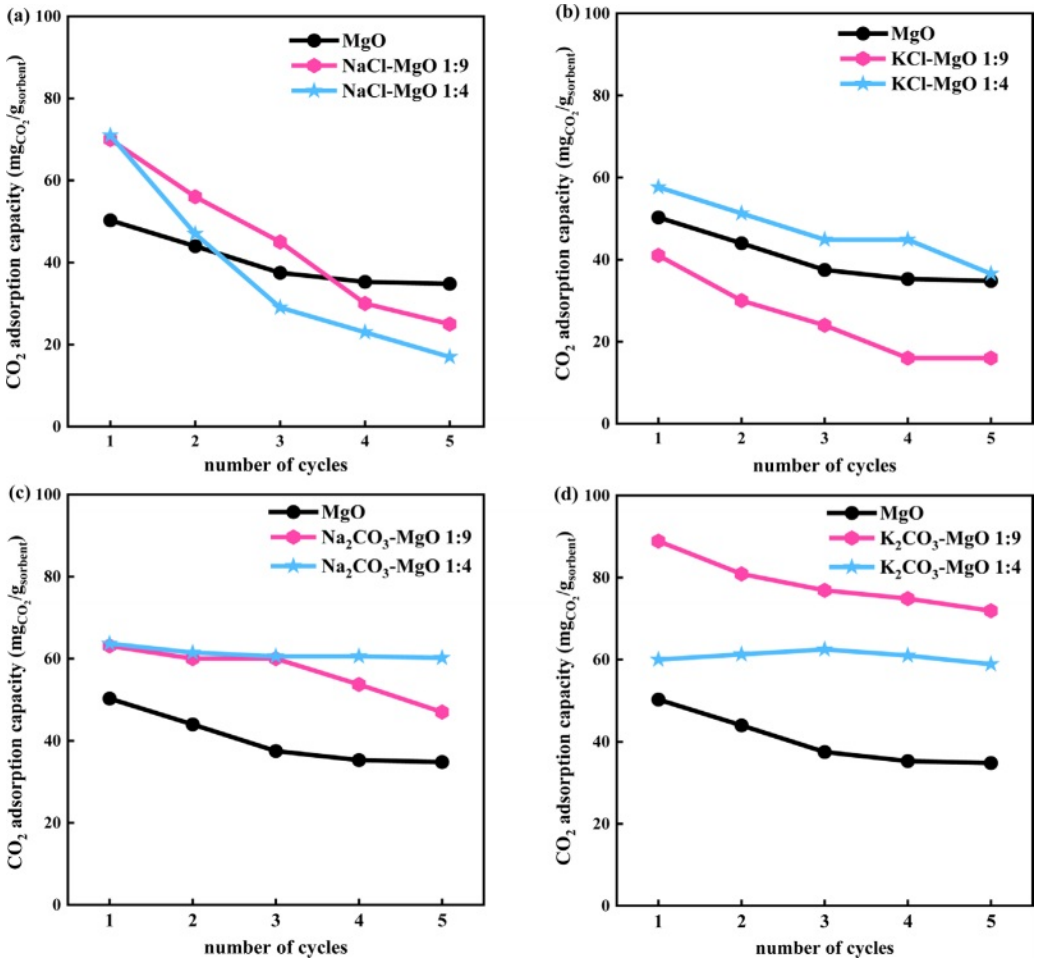

Fig. 3. Comparison of adsorption capacity of MgO based adsorbents modified with different alkali metal salts (K_2CO_3, Na_2CO_3, KCl, NaCl) at 380°C.

mg/g·adsorbent and 60.2 mg/g·adsorbent. Therefore, adding alkali metal carbonates (K_2CO_3, Na_2CO_3) can effectively improve the adsorption performance of MgO based adsorbents for CO_2. Especially for MgO based adsorbents with a mass ratio of 1:9, the CO_2 adsorption capacity of the adsorbent remains relatively stable after 5 cycles with the addition of alkali metal carbonates. However, the adsorption performance of Na_2CO_3-9MgO adsorbent rapidly decreased after the third cycle. Therefore, three carbonate modified adsorbents with better adsorption performance, namely Na_2CO_3-4MgO, K_2CO_3-9MgO, and K_2CO_3-4MgO, were selected for subsequent characterization analysis and cycling stability research.

Select four adsorbents with better performance for CO_2 adsorption performance research at different temperatures. The CO_2 adsorption capacities of K_2CO_3-9MgO, K_2CO_3-4MgO, Na_2CO_3-9MgO, Na_2CO_3-9MgO and MgO at different temperatures (280°C, 330°C and 380°C) were investigated. The results are shown in Fig. 4. It can be seen from the figure that temperature has obvious influence on the adsorption capacity of adsorbent CO_2. In a certain temperature range, the adsorption capacity of adsorbent with the same cycle times will obviously increase with the increase of adsorption temperature [14-16]. At 280°C, K_2CO_3-4MgO and Na_2CO_3-4MgO adsorbents had better adsorption capacity of 60 mg/g·adsorbent and 61 mg/g·adsorbent respectively, while at 330°C and 380°C, K_2CO_3-9MgO adsorbents had better adsorption capacity of 80 mg/g·adsorbent and 89 mg/g·adsorbent respectively.

XRD Analysis

The XRD spectra of the fresh and the 15 cycles of adsorbents are shown in Figs. 5 and 6. The diffraction peaks of MgO were observed in XRD patterns of all adsorbents. $Mg(OH)_2$ diffraction peaks are present in fresh adsorbent samples which may be the reason for the existence of water vapor in the air.

The XRD pattern of the fresh Na_2CO_3-4MgO shows the crystalline phase of $Na_2Mg(CO_3)_2$, which is caused by the reaction of Na_2CO_3 and MgO with CO_2. The XRD spectra of K_2CO_3-9MgO and K_2CO_3-4MgO adsorbents show a new phase of $K_2Mg(CO_3)_2$. Lee et al. [17, 18] also mentioned the newly formed substance $K_2Mg(CO_3)_2$, which is the reaction product of MgO,

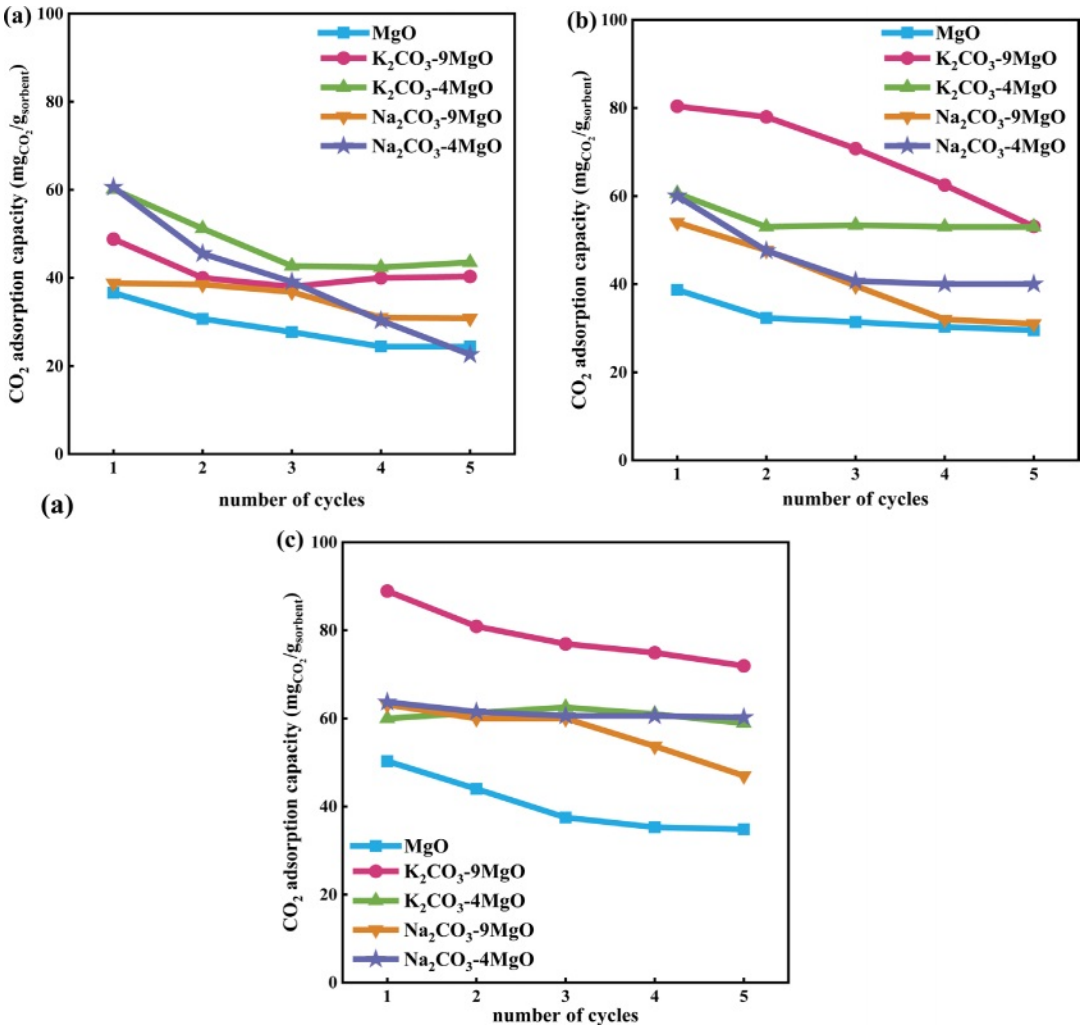

Fig. 4. Comparison of the CO_2 adsorption capacity of different MgO based adsorbent at different temperature: (a) 280°C, (b) 330°C, and (c) 380°C.

K_2CO_3 and CO_2. The existence of $K_2Mg(CO_3)_2$ may be the reason for improving the adsorption performance of the adsorbent. The crystal phase of K_2CO_3 was also detected in K_2CO_3-4MgO adsorbent, which may be the reason why the adsorption performance of K_2CO_3-4MgO adsorbent is lower than that of K_2CO_3-9MgO adsorbent.

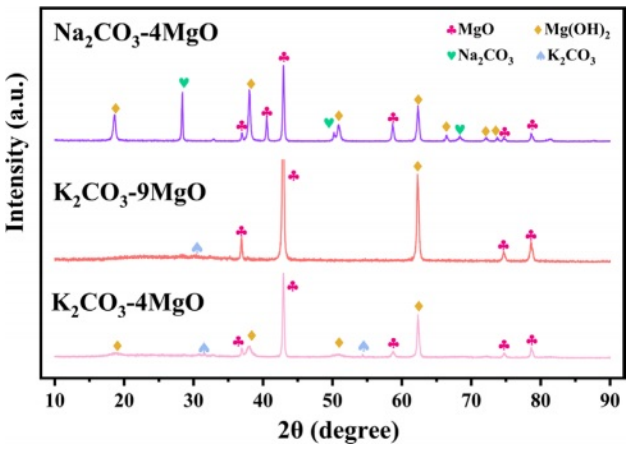

Fig. 5. XRD pattern of the fresh adsorbents.

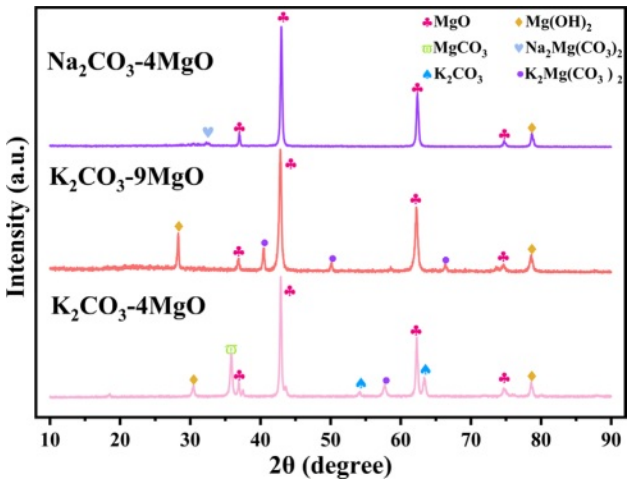

Fig. 6. XRD pattern of different adsorbents after 15 cycles.

SEM and EDS Analysis

The morphology changes of Na_2CO_3-4MgO, K_2CO_3-9MgO and K_2CO_3-4MgO adsorbents before and after 15 cycles were analyzed by SEM. Fig. 7 is the SEM image of the fresh adsorbent. As shown in the figure, the main body of the nano-flake structure is MgO, and the tiny particles attached to the large layer are doped alkali metal salts. For MgO-based adsorbents modified by alkali metal salts, K_2CO_3-9MgO adsorbents have the thinnest lamellae and more pores.

Figure 8 is the SEM image of the adsorbent after 15 cycles. Compared with fresh adsorbents, the flaky structures of each adsorbent have different degrees of aggregation, which may be the reason for the gradual decline of adsorption performance of adsorbents. At the same time, however, pores with uniform distribution and different sizes are produced on the adsorbent lamellae. This may be due to the chemical reaction between MgO and CO_2 to form $MgCO_3$ during CO_2 adsorption. In the process of cyclic adsorption and release, this reaction may be reversible or partially reversible. Each time magnesium carbonate is formed and decomposed, the crystal structure of MgO may be destroyed, which leads to the change of surface and internal structure of the material and the formation of new holes and cracks [19-21]. Furthermore, during the cycle, the adsorbent adsorbs CO_2 at a relatively low temperature, and then releases CO_2 at a higher temperature. This periodic change in temperature may lead to thermal expansion and contraction of materials, resulting in physical stress. These stresses may lead to the formation of microscopic cracks or holes in the material structure [22-24]. Among them, K_2CO_3-9MgO adsorbent has relatively more pores due to its thinnest layer, and the increase in pores will lead to sufficient contact between the adsorbent and CO_2, which may also be the reason for the better adsorption performance of K_2CO_3-9MgO adsorbent.

Figure 9 shows the surface element distribution of fresh adsorbents Na_2CO_3-4MgO, K_2CO_3-9MgO and K_2CO_3-4MgO. It can be found that Mg, O, Na, C and K elements on the surface of MgO-based adsorbent modified by alkali metal salt prepared by this method are uniformly distributed. Especially for K_2CO_3-9MgO adsorbent, in which doped alkali metal salts are uniformly distributed among MgO lamellae, effectively inhibiting the formation of $MgCO_3$ layer during cyclic calcination, therefore K_2CO_3-9MgO adsorbent can still keep thin lamellae structure and obtain higher CO_2 adsorption capacity after multiple cycles.

BET Analysis

Typical BET isotherms and corresponding pore size distribution curves for various samples are shown in Figs. 10 and 11. Due to the best adsorption and cycling performance of K_2CO_3-9MgO adsorbent in this experiment, this study compared the N_2 adsorption-desorption curves and pore size distribution curves of fresh Na_2CO_3-4MgO, K_2CO_3-9MgO, and K_2CO_3-4MgO adsorbent samples and K_2CO_3-9MgO adsorbent samples after 15 cycles. It was found that K_2CO_3-9MgO adsorbent has the smallest pore size among the fresh adsorbents, which may be the reason for its best adsorption performance.

At the same time, it can be observed that the pore size of K_2CO_3-9MgO adsorbent will increase after 15 cycles. The pore size of fresh adsorbents is mainly distributed between 0-15 nm. After 15 cycles, the pore size of K_2CO_3-9MgO adsorbent is mainly distributed between 10-50 nm. This indicates that the pore size of K_2CO_3-9MgO adsorbent increases during circulation.

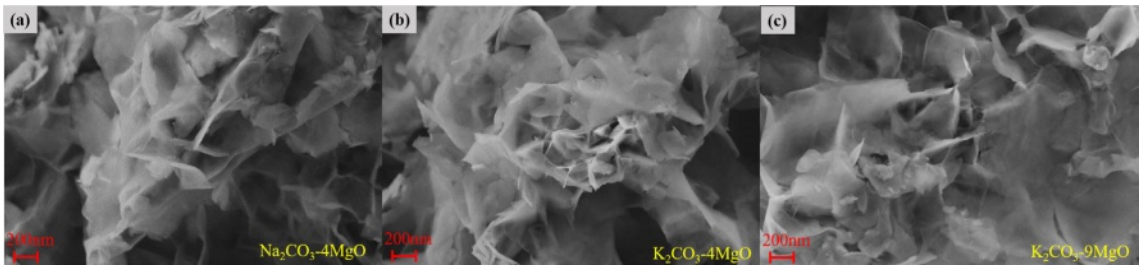

Fig. 7. SEM images of the fresh adsorbents: (a) Na_2CO_3-4MgO; (b) K_2CO_3-4MgO; (c) K_2CO_3-9MgO.

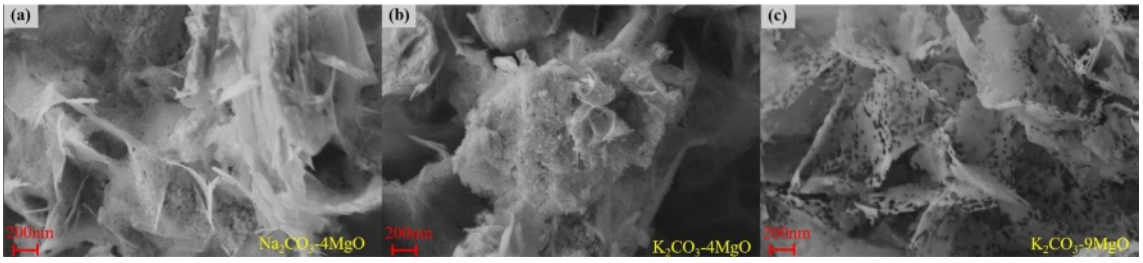

Fig. 8. SEM images of the adsorbents after 15 cycles: (a) Na_2CO_3-4MgO; (b) K_2CO_3-4MgO; (c) K_2CO_3-9MgO.

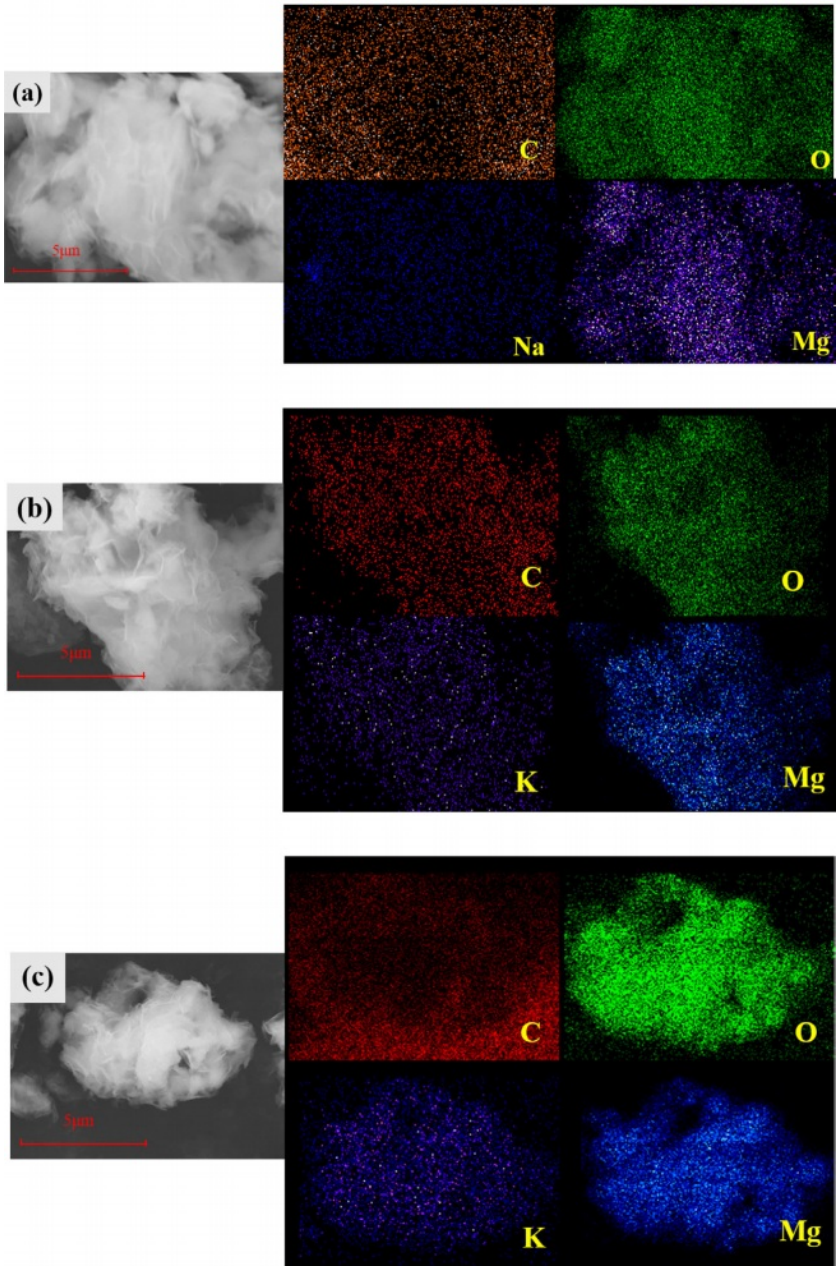

Fig. 9. EDS mapping images of the fresh adsorbents: (a) Na_2CO_3-4MgO; (b) K_2CO_3-4MgO; (c) K_2CO_3-9MgO.

This may be because the crystal structure of MgO may be destroyed during cyclic adsorption and release, and new pores and cracks may be formed. Furthermore, the periodic change of temperature may lead to thermal expansion and contraction of materials, which may lead to the formation of microscopic cracks or holes in the material structure [22-24]. This is consistent with the above SEM characterization results. This is also the reason why the amount of pores distributed between 10-50 nm increases after 15 cycles.

Table 2 shows the pore size, pore volume, and specific surface area of fresh samples of Na_2CO_3-4MgO, K_2CO_3-9MgO, and K_2CO_3-4MgO adsorbents and samples of K_2CO_3-9MgO adsorbents after 15 cycles. It can be seen from the table that K_2CO_3-9MgO adsorbent has the smallest pore size and the largest specific surface area among the fresh adsorbents, which may be the reason for its best adsorption performance. At the same time, it can be seen that after 15 cycles, the pore size of K_2CO_3-9MgO adsorbent will increase, while the pore volume and specific surface area will decrease, which may be the reason for the decline of its adsorption performance [25].

CO_2 Cyclic Adsorption Performance

Three groups of samples (Na_2CO_3-4MgO, K_2CO_3-9MgO and K_2CO_3-4MgO) with good adsorption

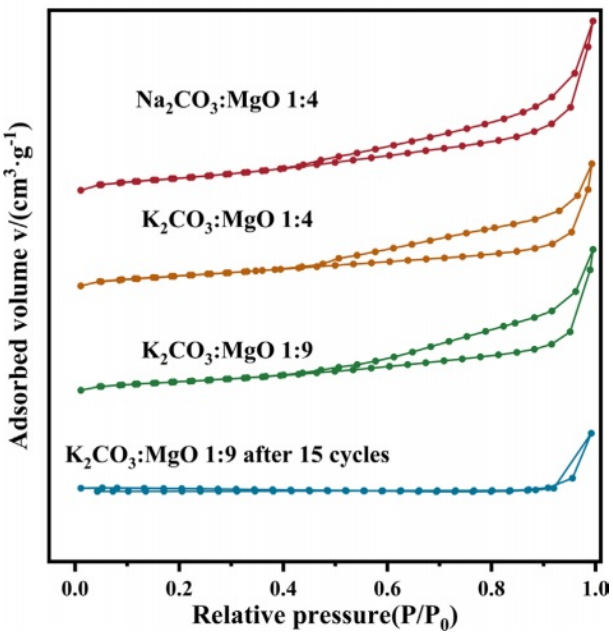

Fig. 10. N_2 adsorption-desorption isotherm linear plot of adsorbents in different states.

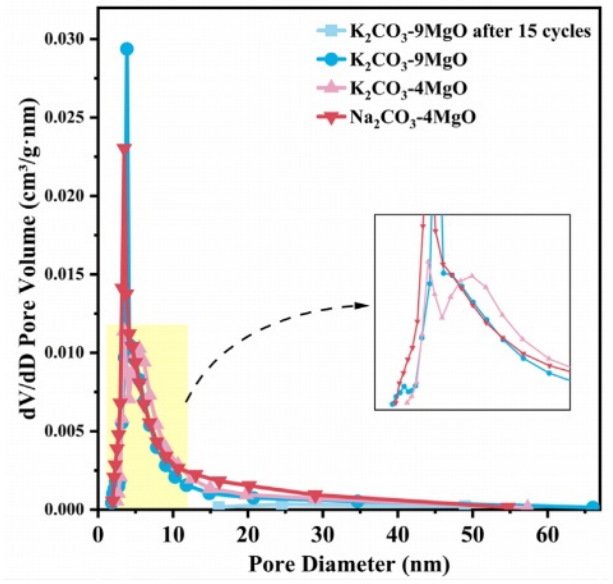

Fig. 11. Pore size distribution of different adsorbents.

performance were selected for multiple cyclic studies. The results are shown in Fig. 12. After 15 cycles, the CO_2 adsorption capacity of K_2CO_3-9MgO adsorbent

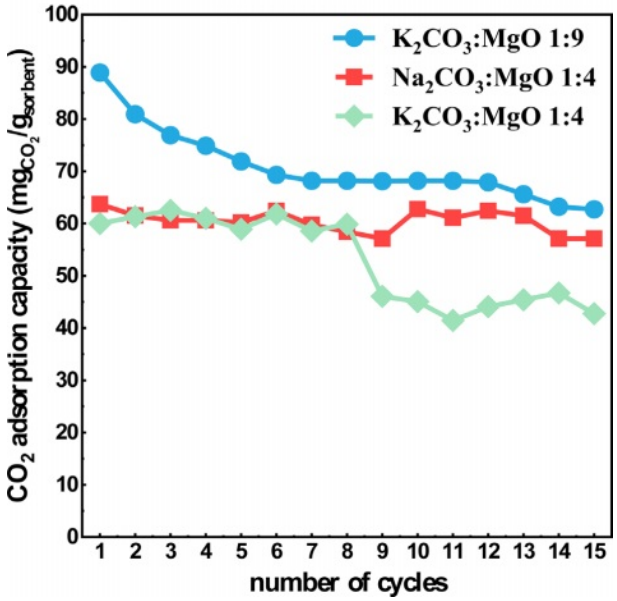

Fig. 12. Comparison of cyclic CO_2 adsorption capacity for15 cycles.

can still reaches at 63 mg/g·adsorbent. This indicates that K_2CO_3-9MgO adsorbent has a relatively stable performance in cyclic CO_2 capture.

Conclusion

In this study, MgO-based adsorbents modified by alkali metal salts with different mass ratios were prepared and applied to capture CO_2 in the atmosphere. The cyclic adsorption capacity of CO_2 was tested in a fixed-bed reactor. XRD, SEM, and BET were used to characterize the physicochemical properties of the adsorbent samples. The influence of alkali metal salt doping on MgO-based adsorbent was deeply studied. The main conclusions are as follows:

Among the 8 modified samples, K_2CO_3-9MgO adsorbent has the largest adsorption capacity, the first adsorption capacity is 89 mg/g·adsorbent, and the adsorption capacity can still reach 63 mg/g·adsorbent after 15 cycles. Compared with other adsorbents prepared in this experiment, the adsorption performance of K_2CO_3-9MgO adsorbent is more ideal and the adsorption capacity is more stable.

The adsorption capacity and cyclic stability of MgO-based adsorbents modified by basic carbonate at different

Table 2. Pore size, Pore volume and specific surface area of the adsorbents.

Adsorbent	Pore size (nm)	Pore volume (cm^3/g)	S_{BET} (m^2/g)
K_2CO_3-9MgO after 15 cycles	38.1393	0.004703	12.9388
K_2CO_3-9MgO	11.2558	0.009957	40.7205
K_2CO_3-4MgO	14.2643	0.000213	36.6374
Na_2CO_3-4MgO	12.7132	0.015970	14.4023

temperatures and different mass ratios were also studied. Overall, the adsorption capacity and cycle stability of modified samples are better than those of unmodified pure MgO-based adsorbents; The performance of K_2CO_3 modified adsorbent is better than that of Na_2CO_3 modified adsorbent. At 330°C and 380°C, the adsorption capacity and cycle performance of K_2CO_3-9MgO adsorbent are the best.

Due to the limitation of research depth, the carbon capture technology explored in this report is mainly based on theoretical research and laboratory verification, and more performance tests are needed to evaluate the practical application of the developed adsorbent in atmospheric CO_2 capture. The purpose of this study is to provide enlightenment for the design of atmospheric CO_2 recycling absorption and adsorption materials with higher efficiency and lower energy consumption. In the future, further work will be carried out to popularize this MgO-based carbon capture technology and apply it to actual carbon capture concentration.

Acknowledgements

This work was supported by the Science and Technology Projects of Liaoning Province (No. 2023JH1/10400077), and the National Natural Science Foundation of China (No. 52001045).

Conflicts of Interest

The authors declare no conflict of interest.

References

1. X. Zhang, Q.W. Shen, K.Y. Zhu, G.K. Chen, G.G. Yang and S.A. Li, J. Mar. Sci. Eng. 11[12] (2023) 2229.
2. Q.W. Shen, Z.C. Shao, Y.H. Jiang, S.A. Li, G.G. Yang, N.B. Huang, and X.X. Pan, J. Ceram. Process. Res. 22[5] (2021) 576-583.
3. S.A. Li, R.Q. Wei, Y.H. Jiang, Q.W. Shen, G.G. Yang and N.B. Huang, J. Ceram. Process. Res. 21[1] (2020) 64-68.
4. Q.W. Shen, Bengt Sunden, G. G. Yang, Y.H. Jiang, and S.A. Li, J. Ceram. Process. Res. 23[5] (2022)611-616.
5. B.W. Jo, J.S. Choi, and S.W. Kang, J. Ceram. Process. Res. 12[3] (2011) 294-298.
6. K.H. Chai, L.K. Leong, S. Sethupathi, K.C. Chong, T.C.K. Yang, S.P. Ong, and Y.H. Yap, Adv. Chem. Eng. 17 (2004) 100578.
7. C. Tan, Y.F. Guo, J. Sun, W.L. Li, J.B. Zhang, C.W. Zhao, and P. Lu, Fuel 278 (2020) 118379.
8. G. Song, X. Zhu, R. Chen, Q. Liao, Y. D. Ding, and L. Chen, Rsc. Advances 6[23] (2016) 19069-19077.
9. A. Hanif, S. Dasgupta, and A. Nanoti, Ind. Eng. Chem. Res. 55[29] (2016) 8070-8078.
10. S.J. Han, Y. Bang, H.J. Kwon, H.C. Lee, V. Hiremath, I.K. Song, and J.G. Seo, Chem. Eng. J. 242 (2014) 357-363.
11. Y.Y. Li, K.K. Han, W.G. Lin, M.M. Wan, Y. Wang, and J.H. Zhu, J. Mater. Chem. A. 1[41] (2013) 12919-12925.
12. G. Xiao, R. Singh, A. Chaffee, and P. Webley, Int. J. Greenh. Gas. Con. 5[4] (2011) 634-639.
13. T. Harada, F. Simeon, E.Z. Hamad, and T.A. Hatton, Chem. Mater. 27[6] (2015) 1943-1949.
14. C.A. del Pozo, S. Cloete, J.H. Cloete, Á.J. Álvaro, and S. Amini, Energy Convers. Manage. 201 (2019) 112109.
15. K. Palle, S. Vunguturi, K. Subba Rao, S. Naga Gayatri, P. Ramesh Babu, M. Mustaq Ali, and R. Kola, Chem. Pap. 76[12] (2022) 7865-7866.
16. X. Li, W. Shen, H. Sun, L. Meng, B. Wang, C. Zhan, and B. Zhao, RSC Advances 10[53] (2020) 32241-32248.
17. K.B. Lee, M.G. Beaver, H.S. Caram, and S. Sircar, Ind. Eng. Chem. Res. 47[21] (2008) 8048-8062.
18. S.C. Lee, H.J. Chae, S.J. Lee, B.Y. Choi, C.K. Yi, J.B. Lee, and J.C. Kim, Environ. Sci. Technol. 42[8] (2008) 2736-2741.
19. D.G. Madden, H.S. Scott, A. Kumar, K.J. Chen, R. Sanii, A. Bajpai, and M.J. Zaworotko, Phil. Trans. R. Soc. A 375[2084] (2017) 20160025.
20. A.N. Stuckert and R.T. Yang, Environ. Sci. Technol. 45[23] (2011) 10257-10264.
21. G. Li, P. Xiao, P. Webley, R.S. Zhang, and M. Marshall. Adsorption 14 (2008) 415-422.
22. A.M. Pinto, I.C. Goncalves, and F.D. Magalhaes, Colloid. Surface. B. 111 (2013) 188-202.
23. S.Y. Lee and S.J. Park, J. Ind. Eng. Chem. 23 (2015) 1-11.
24. L.K.G. Bhatta, S. Subramanyam, M.D. Chengala, S. Olivera, and K.J. Venkatesh, J. Clean Prod. 103 (2015) 171-196.
25. B. Li, Y. Li, H. Sun, Y. Wang, and Z. Wang, Energy & Fuels 34[5] (2020) 6462-6473.